Solid phosphoric acid catalysts based on mesoporous silica for levoglucosenone production via cellulose fast pyrolysis

J. A. Santander [a]*, M. Alvarez [a], V. Gutierrez [b], M. A. Volpe [b].

[a] Instituto de Química del Sur, INQUISUR (CONICET-UNS), Av. Alem 1253, Bahía Blanca (8000), Argentina.

[b] Planta Piloto de Ingeniería Química, PLAPIQUI (CONICET-UNS), Florida 7500, Bahía Blanca (8000), Argentina

*Corresponding author, José A. Santander, e-mail address: jose.santander@uns.edu.ar, phone number: +54 0291 4595101 ext. 3592

Abstract

BACKGROUND:

Biochemicals are interesting alternatives for biomass valorization owing to their much higher added value compared to biofuels and energy products. Several methods for the production of valuable chemicals such as levoglucosenone (LGO) via thermochemical processes over solid acid catalysts are being investigated due to their important advantages compared to conventional biomass acid impregnation techniques. The present work explores the synthesis of catalytic materials for the production of this platform molecule.

This article has been accepted for publication and undergone full peer review but has not been through the copyediting, typesetting, pagination and proofreading process, which may lead to differences between this version and the Version of Record. Please cite this article as doi: 10.1002/jctb.5795

RESULTS:

Aluminum-loaded SBA-15 mesoporous silica and the corresponding solid phosphoric acid catalysts were prepared, characterized by TEM, FT-IR, MAS NMR, NH_3-TPD, N_2 adsorption, ICP-AES and titration of "free H_3PO_4", and tested in cellulose fast pyrolysis. Post synthesis Al deposition on the silica support produced an increase of bio-oil yield and LGO amount in pyrolysis products. The presence of Al in solid phosphoric acid (SPA) catalysts led to the formation of aluminum phosphates, decreasing the concentration of H_3PO_4 species in the surface and therefore the LGO levels. The SPAs presented relatively high LGO levels in the GC-MS detectable liquid products (up to 85 peak area%) which was found to be correlated with the amount of free H_3PO_4 in the solid catalysts.

CONCLUSION:

Aluminum grafting over SBA-15 is an effective way to increase the selectivity to the target anhydrosaccharide. In SPAs, the presence of Al reduced the easily leachable H_3PO_4 amount, which is desirable from the point of view of catalyst stability since deactivation is mainly caused by H_3PO_4 leaching, but also led to lower levels of LGO in bio-oil.

KEYWORDS: Solid phosphoric acid, cellulose pyrolysis, levoglucosenone, mesoporous silica, aluminum grafting.

Introduction

Biomass-derived chemicals are attractive commercial possibilities owing to their much higher added value compared to fuels and energy products in the context of an optimized production of chemicals, power and biofuels in a biorefinery.[1] Levoglucosenone (LGO; 1,6-anhydro-3,4-dideoxy-β-D-glycero-hex-3-enopyranose-2-ulose) is a valuable chemical that has been used as a building block for the synthesis of a wide variety of pharmaceuticals, natural products and rare carbohydrates.[2,3,4] The hydrogenated form of LGO, dihydrolevoglucosenone (Cyrene), is useful as a bio-based polar, aprotic solvent with the potential to replace petrochemical-derived NMP and similar solvents in synthetic chemistry and other applications.[5] LGO can be selectively produced from cellulose pyrolysis. Levoglucosenone can also be conveniently obtained via pyrolysis of phosphoric acid-treated newsprint and other waste papers as cellulose-containing raw materials.[4,6,7] Considering that paper products are one of the main components in municipal solid wastes,[8] industrial production of this useful and valuable chiral building block from available waste cellulosic material could solve some environmental problems and be classified as green chemistry.[9] High concentration of levoglucosenone in the liquid products can be achieved via impregnation of cellulose-containing raw materials with mineral acids or ionic liquids prior to pyrolysis.[10,11] An alternative approach to producing this anhydrosugar from cellulose is to use polar aprotic solvents such as THF and sulfolane.[12,13] Relatively high yields of LGO can be obtained with these methods (up to 51% on a molar basis). Important issues to take into account when considering the use of the

previously described methods are the requirement of less reusable or non-reusable chemicals, the slow reaction in solvents and the need of pretreatments of cellulose in acid impregnation methods, in the latter case the impregnation of biomass with liquid acids is not desirable from an environmental point of view. In this context, solid acid catalysts appear as a promising alternative. In this type of catalysts; e.g., zeolites, mixed metal oxides, mounted acids, mesoporous materials, the surfaces of solids act as acids under reaction conditions. Solid acid catalysts present several advantages when compared to homogeneous catalytic substances, including the feasibility of a continuous production, higher reaction temperatures, simple separation of the catalyst from the reaction mixture and the possibility of regeneration for recycle use.[14] Moreover, solid acid catalysts are not corrosive.

Among the different solid acid catalysts, supported acids consist of an acid spread over the surface of a carrier material. When the mineral acid used to impregnate the support is phosphoric acid, the resulting solid is called Solid Phosphoric Acid (SPA). SPAs are efficient industrial catalysts for processes such as ethylene hydration to ethanol, alkylation of benzene with propene to cumene and oligomerization of propene and isobutene to produce gasoline components.[14] Zhang et al.[15] explored the production of levoglucosenone from catalytic fast pyrolysis of biomass mechanically mixed with SPA catalysts. The obtained LGO yields, particularly for H_3PO_4-impregnated SBA-15 mesoporous silica, were higher than the yields reported in literature for different kinds of solid acid catalysts such as solid superacids (e.g. sulfated metal oxides [16,17]) and bare metal oxides (namely, zirconia, titania, and alumina [18]), and comparable with nanopowder metal oxides.[19,20]

In the present study, solid phosphoric acid catalysts based on aluminum-grafted SBA-15 mesoporous silica were prepared, characterized and tested in cellulose fast pyrolysis towards LGO production. It is known that aluminum incorporation to mesoporous silica materials of the MCM-41 type produces an increase in acidity of the support, enhancing in this way the bio-oil yield and LGO levels in pyrolysis products.[21,22] The aim of this work is to evaluate the effect of the incorporation of variable amounts of aluminum on the structure and catalytic performance of SBA-15 mesoporous silica as well as the influence of Al presence in solid phosphoric acid catalysts. Issues related to stability under reaction conditions are also assessed.

Experimental

Catalysts preparation

Aluminum loaded SBA-15 catalysts were prepared by post-synthetic grafting method. Commercial SBA-15 mesoporous silica (Aldrich, 99%) was grafted with aluminum isopropoxide $Al(OC_2H_7)_3$ (Aldrich, 98%). The Si/Al molar ratios varied from 10 to 50. In a typical procedure, the desired amount of the alkoxide was dissolved in 30 mL of n-hexane (Merck, 99%) and the resulting solution was stirred vigorously for 12 h. Then, 1 g of SBA-15 was added gradually to the solution under continuous stirring and the slurry was stirred for 12 h. After filtration, the solid product was washed repeatedly with n-hexane, dried at room temperature for 24 h and calcined at 400 °C for 2 h in air. The Al-containing SBA-15 catalysts were denoted as Al/SBA-15(y), where "*y"* refers to the Si/Al molar ratio.

Solid phosphoric acid catalysts were prepared by incipient wetness impregnation method according to a procedure described in literature.[15] Typically, 400 mg of the Al/SBA-15 samples or SBA-15 bare support were impregnated with the desired amount of a phosphoric acid aqueous solution in order to obtain a 13 wt% H_3PO_4 concentration in the solid (theoretical elemental phosphorus content of 4 wt%), followed by an ultrasound treatment during 3 h. The catalysts were dried at 80 °C for 12 h and then calcined at 500 °C for 2 h in air. The SPA catalysts were denoted as PO_x/Al/SBA-15(y) and PO_x/SBA-15 for the phosphoric acid impregnated Al/SBA-15(y) and SBA-15 samples, respectively.

Characterization

Metal content was determined by inductively coupled plasma (ICP-AES) on a Shimadzu 9000 simultaneous atomic emission spectrometer.

Specific surface areas were measured by N_2 adsorption at 77 K with a Quantachrome NOVA 1200e apparatus, using the Brunauer-Emmett-Teller (BET) method for the analysis.

Transmission electron microscopy (TEM) images were obtained using JEOL 100 CXII equipment operating at 100 kV. The studies were carried out using magnifications between 10000x and 270000x. Prior to the analysis, the samples were dispersed in ethanol using a sonicator.

Infrared spectra of the catalysts were recorded at room temperature on a Thermo Scientific Nicolet iS50 FT-IR spectrometer, working in the 4000‑400 cm^{-1} wavenumber range at a resolution of 4 cm^{-1} and by averaging over 64 scans. The

samples were pre-treated at 400 °C during 2 h in air before being pressed into self-supporting wafers (2 wt% catalyst in KBr) and placed in a sample holder. Net infrared spectra were obtained by subtracting the sample background spectrum from the whole spectrum.

Solid-state ^{27}Al and ^{31}P magic angle spinning nuclear magnetic resonance (MAS NMR) spectra were recorded at room temperature on a Bruker Avance 300 spectrometer. ^{27}Al MAS NMR spectra were recorded using 1 μs excitation pulse, 1 s repetition time, and 8192 scans. ^{31}P MAS NMR spectra were recorded using 5 μs pulse, 55 s repetition time, and 40 scans. Spinning rate was 10 kHz for all experiments. Chemical shifts of ^{27}Al and ^{31}P were externally referenced to 1M $Al(NO_3)_{3(aq)}$ and $H_3PO_{4(aq)}$, respectively.

Free phosphoric acid percentage was determined by titration of the fraction of phosphoric acids that was leached when the catalyst was first ground into powder and then submerged into room-temperature water for ten minutes.[23] Filtered solution containing the leached phosphoric acids was then titrated with 1×10^{-3} M NaOH aqueous solution. The term "free H_3PO_4" refers to the mass percentage of the titrated H_3PO_4 respect to the total content of phosphoric acid in the samples -as determined by ICP-AES.

The total number of acid sites of the samples was determined by temperature-programmed desorption of NH_3 (NH_3-TPD). Prior to the analysis, the sample (0.050 g) was treated at 300 °C under flowing 10% H_2/N_2 gas mixture (30 mL min^{-1}) for 1 h, then purged for 0.5 h in helium flow and cooled down to room temperature in the same inert atmosphere. For acidity measurements, adsorption of ammonia was performed with a 10% NH_3 in He stream (20 mL min^{-1} flowrate) for 1 h, followed by

a purge for 0.5 h in flowing helium (30 mL min^{-1}). Then, the sample temperature was increased from 30 to 700 °C at a rate of 10 °C min^{-1} under helium gas flow. The amount of evolved NH_3 was measured using thermal conductivity detector (TCD).

Reaction tests

Cellulose pyrolysis experiments were performed on a laboratory scale fixed-bed reactor (see Figure 1). In a usual procedure, 500 mg of high purity microcrystalline cellulose (purchased from Biopack) were mechanically mixed with 75 mg of solid catalyst (15 wt% catalyst in the feedstock) and subsequently supplied to the preheated reaction medium. The reactor consisted of a vertically arranged glass tube of 15 mm internal diameter which was heated externally by an electrical resistance. When the desired temperature was reached (325 °C for all experiments), the mixture of catalyst and cellulose was dropped into the glass tube where an appropriate amount of glass fiber was placed as a support. Reaction time was 15 min for all experiments. At the reactor outlet, the vapors were collected in a condenser cooled by an ice bath. Nitrogen was used as an inert gas, supplied at 150 cm^3/min flowrate.

[Figure 1]

The condenser was weighted before and after pyrolysis in order to determine the liquid products amount produced in the reaction. Bio-oil was diluted with

acetonitrile (Aldrich, 99,8%) in order to obtain a 3 wt% concentration. Liquid products were analyzed by gas chromatography coupled to mass spectrometry (GC-MS). The analyses were performed on an Agilent 7890B gas chromatograph connected to an Agilent 5977 quadrupole mass spectrometer. Analytes were separated by an HP-5 (Agilent) fused-silica capillary column (stationary phase poly(5% diphenyl/95% dimethyl)siloxane, 30 m, 0.25 mm i.d., 0.25 µm film thickness). Helium was used as a carrier gas, with a split ratio of 1:20 and a constant flowrate of 1.0 mL/min. Detector and injector temperature were maintained at 160 °C and 280 °C, respectively. Mass spectra were recorded under electron ionization at 70 eV within the m/z 35–400 range. GC–MS analysis was performed with the follow temperature program: The GC oven was initially maintained at 65 °C for 5 min, followed by a 10 °C/min ramp to 280 °C (held for 10 min). Bio-oil was and dissolved in 4.75 mL of acetonitrile prior to analysis and 1 µL was injected into the injection port. The chromatographic peaks were identified according to the NIST library. LGO peak area% was calculated as the percentage of peak area respect to the total area of peaks in the mass chromatogram. In order to clearly identify trends in the experimental values, data points resulting from pyrolysis tests were fitted with B-spline functions available in the data analysis software.

Results and discussion

Chemical composition and textural properties

The elemental composition of the calcined materials is presented in Table 1. In all cases, the Si/Al molar ratio determined by ICP-AES analysis was near the nominal value, indicating that the aluminum added via the alkoxide precursor $Al(OC_2H_7)_3$ was completely incorporated into the solid material after the post-synthesis procedure. The catalysts of the PO_x/Al/SBA-15 series were prepared with the same nominal load of phosphorus, the measured content of this element being in accordance with the expected values.

Table 1. Elemental composition and physicochemical properties of the samples.

Catalyst	Si/Al*	P (wt%)*	Surface area (m^2/g)	^{27}Al MAS NMR		
				Al^{IV} (%)	Al^{V} (%)	Al^{VI} (%)
SBA-15	∞	-	550	-	-	-
Al/SBA-15(10)	10	-	563	30	17	53
Al/SBA-15(20)	17	-	466	30	8	62
Al/SBA-15(30)	30	-	510	37	14	50
Al/SBA-15(50)	47	-	523	39	10	51
PO_x/SBA-15	∞	4.8	291	-	-	-
PO_x/Al/SBA-15(10)	11	5.1	269	15	3	82
PO_x/Al/SBA-15(20)	16	4.9	287	n.d.†	n.d.	n.d.
PO_x/Al/SBA-15(30)	37	4.7	312	n.d.	n.d.	n.d.
PO_x/Al/SBA-15(50)	49	4.6	345	n.d.	n.d.	n.d.

***** Determined by ICP-AES
† Not determined

TEM images of the catalysts are shown in Figure 2. Commercial SBA-15 silica mesoporous structure consists of symmetrical pores of cylindrical geometry with a diameter of about 3.5 nm, as seen in Figure 2A.

[Figure 2]

The pores are disposed in a hexagonal arrange, with a center-to-center distance of approximately 9 nm. Figure 2C shows that Al/SBA-15(10) sample presented a uniform distribution of the deposited material and retained the mesoporous structure of the parent SBA-15 support after aluminum deposition, which is desirable from the point of view of accessibility of the reactants during cellulose pyrolysis. Although the impregnation with phosphoric acid produced a reduction in the specific surface area of the silica support (Table 1), the mesopores hexagonal arrange remained unaltered as seen in Figures 2B and 2D.

Characterization of surface structure, aluminum and phosphorus species

The FT-IR spectra of aluminum-modified SBA-15 catalysts are shown in Figure 3. The registered signals are typical of a siliceous material. A very strong band was observed at 1070 cm^{-1} along with a shoulder at 1200 cm^{-1}, attributed to the asymmetric stretching of Si-O-Si bonds.[24,25] Signals at 806 cm^{-1} corresponding to the Si-O-Si symmetrical stretching mode could be identified, while peaks at 455 cm^{-1} were ascribed to bending vibrations of the mentioned bonds.[26,27] It is interesting to note that the 960 cm^{-1} peak corresponding to the Si-OH stretching mode [28,29] decreased in intensity with the addition of aluminum to almost zero for the Al/SBA-15(10) sample. During the post-synthesis treatment, aluminum is incorporated on the mesoporous channels surface via reaction of the Al alkoxide with Si-OH groups; the higher the amount of aluminum added, the lower the concentration of silanol groups remaining at the surface.[30,31] An analogous effect

occurred after impregnation with phosphoric acid and subsequent calcination where a decrease in the intensity of the band centered at 960 cm^{-1} was also observed. It is known the interaction between H_3PO_4 and the surface isolated OH groups on mesoporous silica and zeolite materials after post-synthesis treatments.[32,33] During calcination, P–O–Si bonds are formed by dehydration, thus phosphorus species are grafted onto the surface and the concentration of Si–OH groups decrease. It is worth mentioning that the reduction in the amount of surface silanol groups due to their interaction with H_3PO_4 leads to an improvement in the hydrothermal stability of the mesoporous framework by minimizing the hydrolysis of Si–OH groups by water molecules.[34]

[Figure 3]

Solid-state ^{27}Al MAS NMR spectra of the Al/SBA-15 catalysts series presented three signals at -3, 28 and 50 ppm attributed to aluminum atoms with octahedral (Al^{VI}), pentahedral (Al^{V}) and tetrahedral (Al^{IV}) coordination, respectively (Figure 4A). The Al^{IV} peak (50 ppm) exhibited a chemical shift different from that corresponding to bulk Al_2O_3 phase (65 ppm) suggesting both the formation of Al-O-Si bonds during post-synthesis treatment and a possible incorporation of aluminum atoms into the silica network.[30] The success of the grafting process could be evidenced by the relative proportion of the tetra-coordinated and hexa-coordinated species of aluminum. In samples containing only Al_2O_3 phase, 70-80% of the Al atoms resides at octahedral sites, while 20-30% are found in tetrahedral coordination.[35] Conversely, the relative amounts of Al^{IV} and Al^{VI} were not so

different for the Al/SBA-15 samples where the concentration of the Al species varied between 30 to 40% for tetra-coordinated aluminum and from 50 to 60% for hexa-coordinated aluminum (see Table 1). On the other hand, the presence of significant amounts of penta-coordinated Al supported the previous observation since the concentration of Al^V species in pure alumina is quite limited.[35] The aluminum atoms with pentahedral coordination have been suggested to be present as a highly disordered interface connecting a silica or silica-alumina domain with an alumina domain.[36] The shoulder at 65-70 ppm can be attributed to the Al_2O_3 domain.

[Figure 4]

After the addition of phosphorus, the appearance of new signals in the ^{27}Al MAS NMR spectrum evidenced the formation of Al-O-P bonds (see Figure 4A), whereas the intensity of Al peaks observed before impregnation with H_3PO_4 was strongly reduced. Phosphoric acid interacted with aluminum species regardless of their coordination state to form aluminum phosphates. It has been reported that the strong interaction of H_3PO_4 with Al can even lead to the dealumination of H-ZSM-5 zeolites framework after an impregnation with phosphoric acid and a subsequent thermal treatment.[33] The new asymmetric signal at 36 ppm corresponds to Al nuclei tetrahedrally coordinated, while an intense signal appeared at -19 ppm attributed to 6-fold coordinated aluminum. A weak peak at 6 ppm suggests the presence of penta-coordinated aluminum.[37]

A sharp signal at -0.6 ppm could be identified in the ^{31}P MAS NMR spectra of the phosphoric acid-impregnated silica, PO_x/SBA-15, corresponding to monomeric $[PO_4]^{3-}$ groups similar to those present in orthophosphoric acid [33] (Figure 4B). The nature of phosphoric acid is not modified when impregnated on the pure silica substrate.[38] According to the ^{31}P MAS NMR spectrum of the PO_x/Al/SBA-15(10) sample, there is an evident interaction between phosphoric acid and the Al-loaded support verified by the drastic reduction of the signal at -0.6 ppm corresponding to orthophosphates and the appearance of a broad band centered at -21 ppm attributed to aluminum phosphates.[37,39] The phosphorus signal at ca. -22 ppm can be assigned to phosphorus atoms bonded to four- and five-coordinated aluminum species. The shoulder at -28 ppm indicates that part of aluminum in the second coordination shell of phosphorus is tetrahedrally coordinated.[37] This is in line with the ^{27}Al MAS NMR spectra of PO_x/Al/SBA-15(10), where four-, five- and six-fold coordinated Al species were detected.

Acidity characterization

The free H_3PO_4 determination involves the quantification by titration of the phosphoric acid leached from the catalyst when submerged in water. The free H_3PO_4 amount provides an indication of the condensation degree of the phosphoric acids in the catalyst -i.e., ortho-, pyro-, tri- and polyphosphoric acids, with increasing condensation degrees- after the calcination process. The acids with lower condensation degree; namely, ortho- and pyro-phosphoric acids, are easily hydrolyzed and thus can be titrated.[23] This method has also been used to

estimate the strength of the interactions between a given support and the deposited H_3PO_4.[40] In the present study, free H_3PO_4 has been found to be related to the phosphoric acid amount that has not interacted with the aluminum of the support during the synthesis. Table 2 shows that the amount of free phosphoric acid decreases with increasing Al content. As previously described, aluminum strongly interacts with H_3PO_4 to form Al phosphates producing a modification in the amount of titratable H_3PO_4. The higher the aluminum content, the lower the amount of phosphoric acid available for titration, and as a result a decrease in the free H_3PO_4 percentage is observed.

Table 2. Acidic properties of the Al/SBA-15 and PO_x/Al/SBA-15 materials.

Sample	Free H_3PO_4 (%)†	Total acidity ($mmol_{NH3}/g_{cat}$)
SBA-15	-	1.171
Al/SBA-15(10)	-	1.335
Al/SBA-15(20)	-	1.456
Al/SBA-15(30)	-	1.342
PO_x/SBA-15	5.0	1.582
PO_x/Al/SBA-15(10)	0.7	1.430
PO_x/Al/SBA-15(20)	2.6	1.270
PO_x/Al/SBA-15(30)	6.8	1.540
PO_x/Al/SBA-15(50)	7.2	1.554

† Percent amount of leached H_3PO_4 respect to the total content of phosphoric acid in the samples.

Total acidity of the solids was determined through ammonia temperature-programmed desorption experiments. The amount of desorbed NH_3 was higher for the Al/SBA-15 catalysts when compared to the bare SBA-15 support (see Table 2). It is well known that the incorporation of aluminum via post-synthesis treatment

produces an increase in acidity of SBA-15 mesoporous silica.[30,41,42,43,44] Phosphoric acid impregnation of untreated SBA-15 sample also led to an increase in total acidity. The highest amount of desorbed ammonia was observed for POx/SBA-15 sample, which can mainly be attributed to Brønsted acid sites.[45]

Reaction tests

The Al/SBA-15 catalysts series and the PO_x/Al/SBA-15 solid phosphoric acid catalysts were tested in cellulose fast pyrolysis for levoglucosenone production. The main volatile reaction products were 1,6-anhydro-3,4-dideoxy-β-D-glycero-hex-3-enopyranose-2-ulose (levoglucosenone; LGO), 1,6-anhydro-β-D-glucose (levoglucosan, LG), 1,4:3,6-dianhydro-α-D-glucopyranose (DGP) y furan-2-carbaldehyde (furfural). A detailed list of the identified compounds as well as their percentage in detectable liquid products can be found in the Supplementary Material. Figure 5 shows total ion chromathograms of samples modified with aluminum and phosphorus.

[Figure 5]

The first stage in cellulose fast pyrolysis is the depolymerization to oligosaccharides, followed by the cleavage of the β-1,4-glycosidic bonds and the further formation of glucopyranose and other products.[46] According to the detected reaction products, a possible reaction scheme for bio-oil formation is shown in Figure 6.

[Figure 6]

The dehydration and decomposition of the D-glucopyranose units lead to the formation of anhydromonosaccharides (namely, LG, LGO, DGP) and furans (mainly furfural), respectively. Regarding the products distribution for the Al/SBA-15 catalysts, Figure 7 shows that the LGO area percent rises markedly as the aluminum content increases. An opposite trend was observed for levoglucosan with decreasing Si/Al ratio. Since pyrolysis conducted on an acidic environment proceeds via catalysis of hydrolytic depolymerization and dehydration reactions,[47] the higher amount of acidic sites generated on the catalyst surface by aluminum deposition promotes the dehydration reactions, and hence the levoglucosenone formation at the expense of LG. This reaction pathway has been proposed for acid-catalyzed cellulose pyrolysis [46,48] without excluding the possibility of DGP behaving also as a precursor of levoglucosenone.[49,50]

Furfural proportion increased with decreasing Si/Al ratios. The higher concentration of acid sites after Al deposition promoted the decomposition of cellulose to furans. The slight increase in furfural amount can also be related to the enhanced production of LGO, given that such furan is a product of the pyrolysis of levoglucosenone under acidic environment.[51]

DGP peak area% does not have a definite tendency since it rises with decreasing Si/Al ratios at low aluminum contents and presents the opposite trend when the amount of Al is high. The role of intermediary of this dianhydro sugar has been observed in acid catalyzed pyrolysis reactions.[49] While the formation of the 3,6-

anhydo ring of DGP from the dehydration of D-glucopyranose is catalyzed by acids, the decomposition of DGP is also favored in acidic conditions.

Finally, the higher aluminum content produced a slight increase in bio-oil yield (Figure 8) because of an enhanced cellulose depolymerization.

[Figure 7]

[Figure 8]

Concerning the reaction experiments conducted over the phosphoric acid-impregnated catalysts, Figure 9 shows that the proportion of each product exhibits an opposite behavior to that observed for the Al/SBA-15 samples. The latter phenomenon seems to be related to the decrease in free H_3PO_4 levels as the Si/Al ratio decreases on the SPA catalysts (Table 2). As previously described, aluminum strongly interacts with phosphoric acid producing Al phosphates, thus for the samples with a higher aluminum content there is a lower amount of titratable phosphoric acid; i.e., phosphoric acid leached when submerged in water (free H_3PO_4). The influence of the amount of free H_3PO_4 on the LGO percentage in liquid products and bio-oil yield is presented in Figure 10. A clear correlation can be observed particularly in the first case where levoglucosenone area percent increases as the free phosphoric acid content increases. For reactions catalyzed by acids such as ethylene hydration, it has been found that the presence of free phosphoric acid is a prerequisite for the catalytic activity.[38] The decrease in the activity of the phosphoric acid impregnated zinc oxide/titania, tin oxide/titania,

zirconia and niobic acid carriers was explained by the interactions between the phosphoric acid and those supports. Here, the results suggest that phosphorus species that has not interacted with aluminum –assuming that free H_3PO_4 is related to the amount of those species– catalyze the dehydration reactions that increase the production of LGO as well as the cellulose depolymerization to obtain a greater proportion of liquid products. As the amount of Al is increased in the SPA catalysts, there is a smaller proportion of these phosphoric acid species due to the formation of aluminum phosphates, which leads to a lower bio-oil yield and a modification in the reaction products distribution (see Figures 8 and 9). The lower total acidity presented by POx/Al/SBA-15 samples compared with POx/SBA-15 catalyst is a consequence of the Al-H_3PO_4 interaction and is the main reason for the lower levoglucosenone levels observed in Al-modified SPAs. When the amount of H_3PO_4 available for pyrolysis decreases, dehydration of LG is inhibited; therefore, levoglucosan amount in bio-oil increases. An analogous behavior has been observed in the pyrolysis of cellulose pretreated with variable amounts of phosphoric acid.[10] As the concentration of phosphoric acid in the biomass was increased, there was a higher proportion of LGO compared to LG in the reaction products. The concentration of H_3PO_4 both in the cellulose prior to the pyrolysis and on the surface of the catalyst governs the composition of the products, especially the LG/LGO anhydrosaccharides ratio.

[Figure 10]

It can be noted that the loss of specific surface area after the deposition of phosphoric acid was not a determining factor for bio-oil formation. Despite the 40-50% decrease (see Table 1), the PO_x/Al/SBA-15 catalysts presented a higher yield to bio-oil respect to that of Al/SBA-15 samples. On the other hand, solid phosphoric acid catalysts presented a better performance in LGO production when compared to their non H_3PO_4-impregnated counterparts. Finally, when considering ^{27}Al MAS NMR spectra of Al/SBA-15 catalysts, it wasn´t found any correlation between the relative amounts of different aluminum species and the selectivity towards LGO.

Stability tests

In order to determine the stability of the catalyst in terms of the LGO levels in the volatile products and production of bio-oil, a series of reuse experiments of the PO_x/SBA-15 catalyst were performed. PO_x/SBA-15 was selected for the analysis considering the superior catalytic performance towards the anhydrosaccharide of interest. The sample was subjected to five consecutive pyrolysis tests (Figure 11) with intermediate regeneration stages, which consisted in the calcination of the catalyst and carbon mixture remaining in the reactor at 450 °C under air atmosphere. In the regeneration step, the carbonaceous residues were completely eliminated after a 2h treatment, and the recovered catalyst was used again in a successive pyrolysis run. A fresh make-up catalyst addition of 20% at each stage was necessary to compensate for losses during the recovery procedure.

[Figure 11]

It can be observed that although the percentage of LGO maintained high levels during the tests, a progressive decrease was observed -about 15% at the end of the last experiment. The yield to bio-oil showed a similar behavior, presenting a slight decrease in the course of the tests. The elemental analysis after the fifth consecutive reaction run indicated ca. 25% decrease in the phosphorus content of PO_x/SBA-15 sample (4 wt% for the fresh sample and 3 wt% for the spent catalyst). Free H_3PO_4 measurements after the last experiment showed 80% reduction in titratable phosphoric acid amount, thus indicating that the catalyst loses mainly the phosphoric acid species with low condensation degree. The trends in the products distribution during the stability test of PO_x/SBA-15 showed similarities with those presented by the PO_x/Al/SBA-15 catalysts at increasing aluminum contents; i.e., increasing interaction of Al with the deposited phosphoric acid. These results can be explained by a reduction in the availability of reactive phosphorus species; in the former case, by leaching of the low condensed H_3PO_4 species and in the latter, by an interaction of phosphoric acid with aluminum of the support.

Conclusions

Solid phosphoric acid catalysts based on Al-grafted mesoporous silica were prepared and tested in fast pyrolysis of cellulose. The SBA-15 support retained the hexagonal mesoporous structure after Al-grafting and phosphoric acid treatments. The acidity induced by the Al deposition on the silica support produced an increase of bio-oil yield and levoglucosenone fraction in pyrolysis products. The specific

surface area decrease after the addition of phosphoric acid had no adverse effect either in bio-oil production or in the LGO levels; the highest catalytic activity has been observed in the H_3PO_4-impregnated samples. Phosphoric acid strongly interacted with the Al-containing supports, which was evidenced by the formation of aluminum phosphates. The presence of Al on solid phosphoric acid catalysts led to a lower amount of free H_3PO_4; i.e., the easily leachable phosphoric acid, at the expense of a deterioration in catalytic performance. A clear correlation between the LGO area percent and the amount of free H_3PO_4 was observed, indicating that the fraction of phosphoric acid which has not interacted with aluminum promoted dehydration reactions towards levoglucosenone. Relatively high proportion of LGO was observed in the GC-MS detectable pyrolysis products (about 75-85 peak area% in the mass chromatogram), which is desirable for a simpler isolation of the anhydrosaccharide. In terms of LGO production, Al-free H_3PO_4-loaded SBA-15 catalyst presented the best performance and reasonable stability after successive pyrolysis tests. However, the leaching of phosphoric acid from the catalytic material led to a slight but progressive deactivation and reduction of the LGO fraction in the reaction products.

Acknowledgements

The authors thank Universidad Nacional del Sur and Consejo Nacional de Investigaciones Científicas y Técnicas (CONICET) for the financial support.

References

[1] Crocker M, *Thermochemical conversion of biomass to liquid fuels and chemicals*. Royal Society of Chemistry, Cambridge, pp 178-179 (2010).

[2] Witczak JZ, Levoglucosenone: A Chiral Building Block with a New Perspective, in *Chemicals and Materials from Renewable Resources*, ed by Bozell JJ. American Chemical Society, Washington, pp 81–97 (2001).

[3] Sarotti AM, Zanardi MM, Spanevello RA and Suárez AG, Recent applications of levoglucosenone as chiral synthon. *Curr. Org. Synth.* **9**: 439-459 (2012).

[4] Shafizadeh F, Furneaux RH and Stevenson TT, Some reactions of levoglucosenone. *Carbohydr. Res.* **71**: 169-191 (1979).

[5] Sherwood J, De bruyn M, Constantinou A, Moity L, McElroy CR, Farmer TJ, Duncan T, Raverty W, Hunt AJ and Clark JH, Dihydrolevoglucosenone (Cyrene) as a bio-based alternative for dipolar aprotic solvents. *Chem. Commun.* **50**: 9650 (2014).

[6] Trahanovsky WS, Ochaoda JM, Wang C, Revell KD, Arvidson KB, Wang Y, Zhao H, Chung S and Chang S, A convenient procedure for the preparation of levoglucosenone and its conversion to novel chiral derivatives, in *Carbohydrate synthons in natural products chemistry*, ed by Witczak ZJ and Tatsuta K. American Chemical Society, Washington, pp. 21-31 (2003).

[7] Swenton JS, Freskos JN, Dalidowicz P and Kerns ML, A facile entry into naphthopyran quinones via an annelation reaction of levoglucosenone. The total synthesis of (-)-hongconin, *J. Org. Chem.* **61**: 459-464 (1996).

[8] Chen D, Yin L, Wang H and He P, Pyrolysis technologies for municipal solid waste: A review, *Waste Manage*. **34**: 2466-2486 (2014).

[9] Witczak ZJ and Tatsuta K, *Carbohydrate synthons in natural products chemistry: synthesis, functionalization, and applications.* American Chemical Society, Washington (2003).

[10] Dobele G, Rossinskaja G, Dizhbite T, Telysheva G, Meier D and Faix O, Application of catalysts for obtaining 1,6-anhydrosaccharides from cellulose and wood by fast pyrolysis. *J. Anal. Appl. Pyrolysis* **74**: 401–405 (2005).

[11] Kudo S, Zhou Z, Norinaga K and Hayashi J, Efficient levoglucosenone production by catalytic pyrolysis of cellulose mixed with ionic liquid. *Green Chem.* **13**: 3306 (2011).

[12] Cao F, Schwartz TJ, McClelland DJ, Krishna SH, Dumesica JA and Huber GW, Dehydration of cellulose to levoglucosenone using polar aprotic solvents. *Energy Environ. Sci.* **8**: 1808-1815 (2015).

[13] Kawamoto H, Saito S, Hatanaka W and Saka S, Catalytic pyrolysis of cellulose in sulfolane with some acidic catalysts. *J. Wood Sci.* **53**: 127–133 (2007).

[14] Hattori H and Ono Y, *Solid Acid Catalysis: from fundamentals to applications*. CRC Press, Boca Raton, pp 2-4 (2015).

[15] Zhang Z, Lu Q, Ye X, Wang T, Wang X and Dong C, Selective production of levoglucosenone from catalytic fast pyrolysis of biomass mechanically mixed with solid phosphoric acid catalysts. *BioEnergy Res.* **8**: 1263–1274 (2015).

[16] Wang Z, Lu Q, Zhu X and Zhang Y, Catalytic fast pyrolysis of cellulose to prepare levoglucosenone using sulfated zirconia. *ChemSusChem* **4**: 79–84 (2011).

[17] Lu Q, Ye X, Zhang Z, Dong C and Zhang Y, Catalytic fast pyrolysis of cellulose and biomass to produce levoglucosenone using magnetic SO_4^{2-}/TiO_2–Fe_3O_4. *Bioresour. Technol.* **171**: 10–15 (2014).

[18] Wei X, Wang Z, Wu Y, Yu Z, Jin J and Wu K, Fast pyrolysis of cellulose with solid acid catalysts for levoglucosenone. *J. Anal. Appl. Pyrolysis* **107**: 150-154 (2014).

[19] Fabbri D, Torri C and Mancini I, Pyrolysis of cellulose catalysed by nanopowder metal oxides: production and characterisation of a chiral hydroxylactone and its role as building block. *Green Chem.* **9**: 1374–1379 (2007).

[20] Fabbri D, Torri C and Baravelli V, Effect of zeolites and nanopowder metal oxides on the distribution of chiral anhydrosugars evolved from pyrolysis of cellulose: An analytical study. *J. Anal. Appl. Pyrolysis* **80**: 24–29 (2007).

[21] Torri C, Lesci IG and Fabbri D, Analytical study on the pyrolytic behaviour of cellulose in the presence of MCM-41 mesoporous materials. *J. Anal. Appl. Pyrolysis* **85**: 192–196 (2009).

[22] Casoni AI, Nievas ML, Moyano EL, Álvarez M, Diez A, Dennehy M and Volpe MA, Catalytic pyrolysis of cellulose using MCM-41 type catalysts. *Applied Catalysis A: General* **514**: 235–240 (2016).

[23] Cavani F, Girotti G and Terzoni G, Effect of water in the performance of the “solid phosphoric acid” catalyst for alkylation of benzene to cumene and for oligomerization of propene. *Appl. Catal., A* **97**: 177-196 (1993).

[24] Kokunešoski M, Gulicovski J, Matović B, Logar M, Milonjić SK and Babić B, Synthesis and surface characterization of ordered mesoporous silica SBA-15. *Materials Chemistry and Physics* **124**: 1248–1252 (2010).

[25] Akl MA, Aly HF, Soliman HMA, Abd ElRahman AME and Abd-Elhamid AI, Preparation and Characterization of Silica Nanoparticles by Wet Mechanical Attrition of White and Yellow Sand. *J Nanomed Nanotechnol* **4**: 1-14 (2013).

[26] Bertoluzza A, Fagnano C and Morelli MA, Raman and infrared spectra on silica gel evolving toward glass. *Journal of Non-Crystalline Solids* **48**: 117-128 (1982).

[27] Tran TN, Pham TVA, Le MLP, Nguyen TPT, Tran VM, Synthesis of amorphous silica and sulfonic acid functionalized silica used as reinforced phase for polymer electrolyte membrane. *Adv. Nat. Sci.: Nanosci. Nanotechnol.* **4**: 1-6 (2013).

[28] Azimov F, Markova I, Stefanova V and Sharipov K, Synthesis and characterization of SBA-15 and Ti-SBA-15 nanoporous materials for DME catalysts. *J. Univ. Chem. Technol. Metall.* **47**: 333-340 (2012).

[29] Li J, Guo L and Shi J, Stepwise in situ synthesis and characterization of metallophthalocyanines@mesoporous matrix SBA-15 composites. *Phys. Chem. Chem. Phys.* **12**: 5109–5114 (2010).

[30] Baca M, Rochefoucauld E, Ambroise E, Krafft J, Hajjar R, Man PP, Carrier X and Blanchard J. *Microporous Mesoporous Mater.* **110**: 232–241 (2008).

[31] Gómez-Cazalilla M, Mérida-Robles JM, Gurbani A, Rodríguez-Castellón E and Jiménez-López A, Characterization and acidic properties of Al-SBA-15 materials prepared by post-synthesis alumination of a low-cost ordered mesoporous silica. *J. Solid State Chem.* **180**: 1130-1140 (2007).

[32] Kawi S, Shen SC and Chew PL, Generation of Brønsted acid sites on Si-MCM-41 by grafting of phosphorus species. *J. Mater. Chem.* **12**: 1582–1586 (2002).

[33] Caro J, Bulow M, Derewinski M, Hunger M, Karger J, Kurschner U, Pfeifer H, Storek W and Zibrowius B, NMR characterization of zeolite H-ZSM-5 after post-synthesis modification with H_3PO_4, in *Studies in Surface Science and Catalysis 52: Recent Advances In Zeolite Science*, ed by Klinowski J and Barrie PJ. Elsevier Science Publishers B.V., The Netherlands, pp. 295-304 (1989).

[34] Huang L-M and Li Q-Z, Improvement on thermal stability and acidity of mesoporous materials with post-treatment of phosphoric acid, in *Studies in Surface*

Science and Catalysis 129: Nanoporous Materials II, ed by Sayari A and Jaroniec M, Elsevier Science B.V, pp. 93-98 (2000).

[35] Pecharromán C, Sobrados I, Iglesias JE, González-Carreño T and Sanz J, Thermal Evolution of Transitional Aluminas Followed by NMR and IR Spectroscopies. *J. Phys. Chem. B* **103**: 6160-6170 (1999).

[36] Williams MF, Fonfé B, Sievers C, Abraham A, van Bokhoven JA, Jentys A, van Veen JAR and Lercher JA, Hydrogenation of tetralin on silica–alumina-supported Pt catalysts I. Physicochemical characterization of the catalytic materials. *J. Catal.* **251**: 485–496 (2007).

[37] Mali G, Mazaj M, Rangus M, Soler-Illia GJAA and Kaucic V, Solid-State NMR investigation of formation of mesoporous thin films and powders, in *Zeolites and Related Materials: Trends, Targets and Challenges*, ed by Gédéon A, Massiani P and Babonneau F. Elsevier B.V, Paris, pp. 949-952 (2008).

[38] Fougret CM, Atkins MP and Hölderich WF, Infuence of the carrier on the catalytic performance of impregnated phosphoric acid in the hydration of ethylene. *Appl. Catal., A* **181**: 145-156 (1999).

[39] De Araujo LRR, Scofield CF, Pastura NMR and de Araujo Gonzalez W, H_3PO_4/Al_2O_3 Catalysts: Characterization and Catalytic Evaluation of Oleic Acid Conversion to Biofuels and Biolubricant. *Mater. Res. (Sao Carlos, Braz.)* **9**: 181-184 (2006).

[40] Fougret CM, Atkins MP and Hölderich WF, Influence of the carrier on the catalytic performance of impregnated phosphoric acid in the hydration of ethylene. *Appl. Catal., A* **181**: 145-156 (1999).

[41] Dragoi B, Dumitriu E, Bennici S and Auroux A. Acidic and adsorptive properties of Al modified SBA-15 samples, in *Zeolites and Related Materials: Trends, Targets and Challenges,* ed by Gédéon A, Massiani P and Babonneau F. Elsevier B.V, Paris, pp. 953-956 (2008).

[42] Ma J, Qiang L, Wang J, Tang X and Tang D, Effect of different synthesis methods on the structural and catalytic performance of SBA-15 modified by aluminum, *J. Porous Mater.* **18**: 607–614 (2011).

[43] Hensen EJM, Poduval DG, Magusin PCMM, Coumans AE and van Veen JAR, Formation of acid sites in amorphous silica-alumina. *J. Catal.* **269**: 201–218 (2010).

[44] Gurinov AA, Rozhkova YA, Zukal A, Cejka J and Shenderovich IG, Mutable Lewis and Brønsted acidity of aluminated SBA-15 as revealed by NMR of adsorbed pyridine-^{15}N. *Langmuir* **27**: 12115–12123 (2011).

[45] Ramis G, Rossi PF, Busca G and Lorenzelli V, Phosphoric acid on oxide carriers. 2. Surface acidity and reactivity toward olefins. *Langmuir* **5**: 917-923 (1989).

[46] Wang S and Luo Z, *Pyrolysis of biomass*. De Gruyter, Berlin, pp 62-68 (2017).

[47] Dobele G, Rossinskaja G, Telysheva G, Meier D and Faix O, Cellulose dehydration and depolymerization reactions during pyrolysis in the presence of phosphoric acid. *J. Anal. Appl. Pyrolysis* **49**: 307–317 (1999).

[48] Kawamoto H, Saito S, Hatanaka W and Saka S, Catalytic pyrolysis of cellulose in sulfolane with some acidic catalysts. *J. Wood Sci.* **53**: 127–133 (2007).

[49] Shafizadeh F, Furneaux RH, Stevenson TT and Cochran TG, Acid-catalyzed pyrolytic synthesis and decomposition of 1,4:3,6-dianhydro-α-D-glucopyranose, *Carbohydr. Res.* **61**: 519-528 (1978).

[50] Xia H, Yan X, Xu S, Yang L, Ge Y, Wang J and Zuo S, Effect of Zn/ZSM-5 and $FePO_4$ catalysts on cellulose pyrolysis. *J. Chem.* **2015**: 1-11 (2015).

[51] Shafizadeh F and Chin PPS. Pyrolytic production and decomposition of 1,6-anhydro-3,4-dideoxy- β-D-glycero-hex-3-enopyranos-2-ulose. *Carbohydr. Res.* **46**: 149-154 (1976).

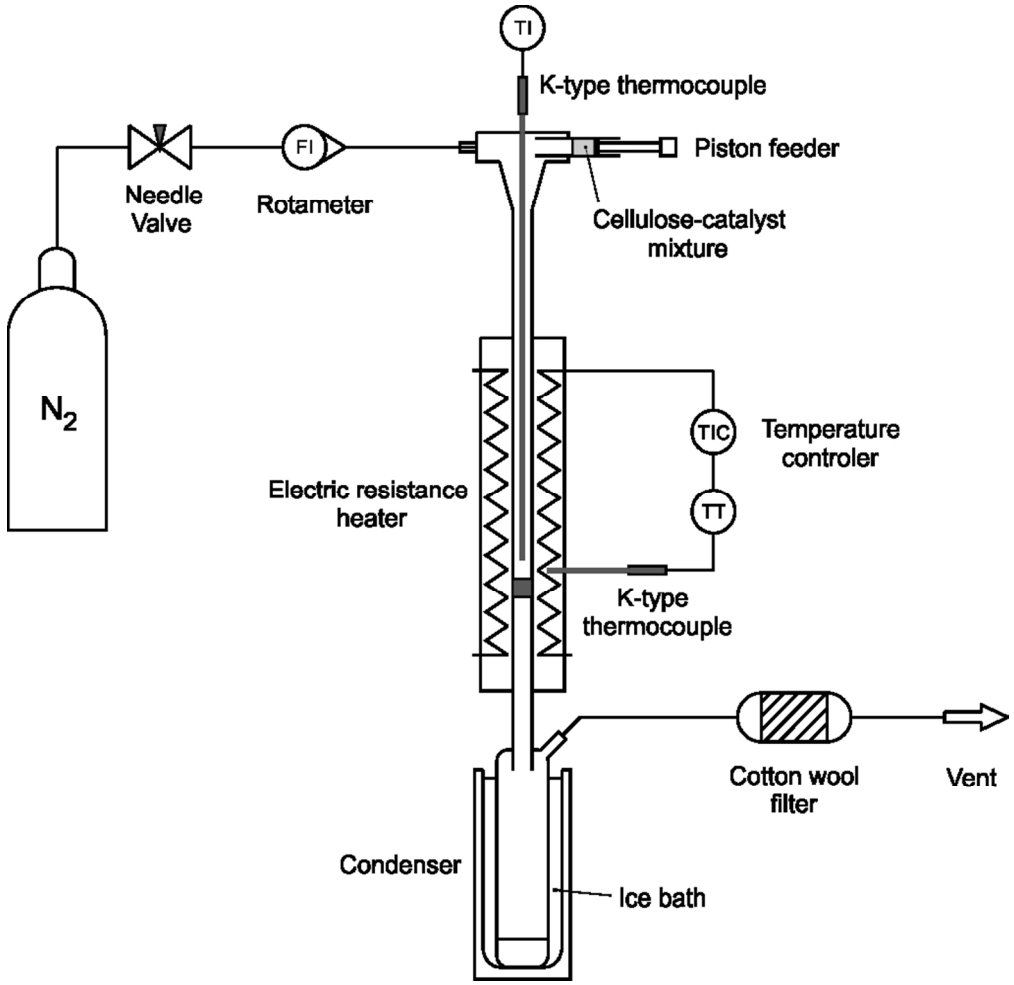

Figure 1. Experimental setup scheme of the pyrolysis reactor.

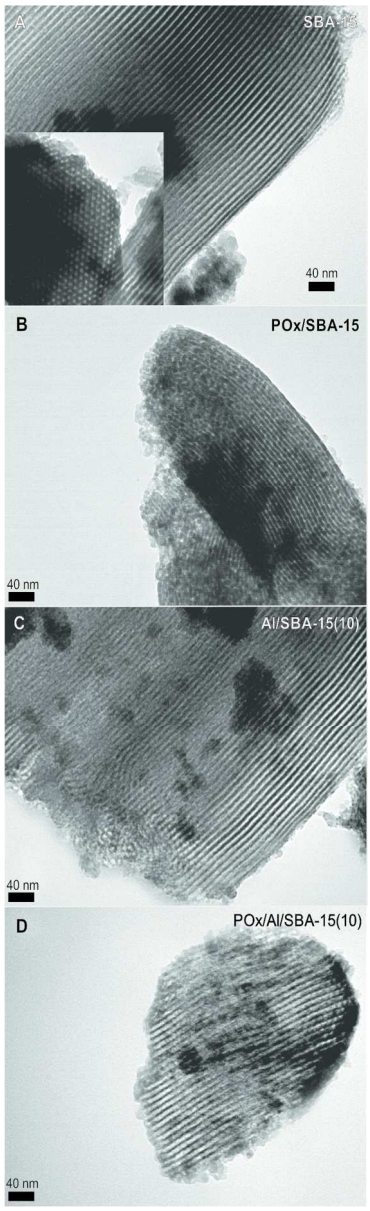

Figure 2. A) TEM micrographs of commercial SBA-15 mesoporous silica, B) SBA-15 support impregnated with phosphoric acid, C) SBA-15 after post-synthesis treatment with Al, D) mesoporous silica support after Al deposition and subsequent H_3PO_4 impregnation.

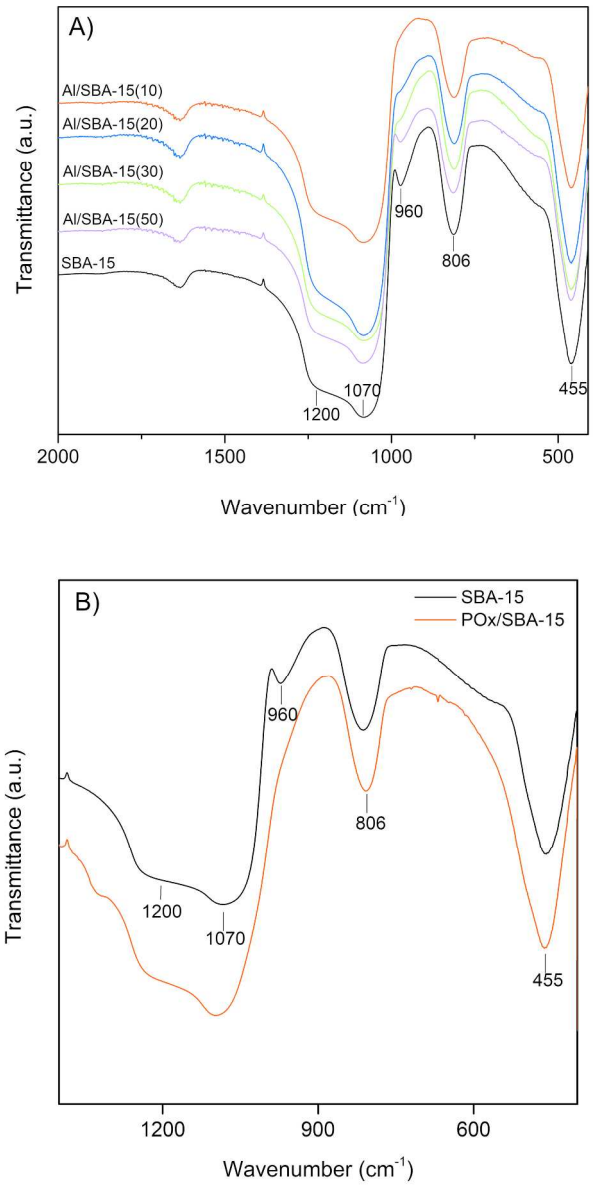

Figure 3. Infrared spectra of A) the Al/SBA-15 catalysts series, B) PO_x/SBA-15 and SBA-15 samples.

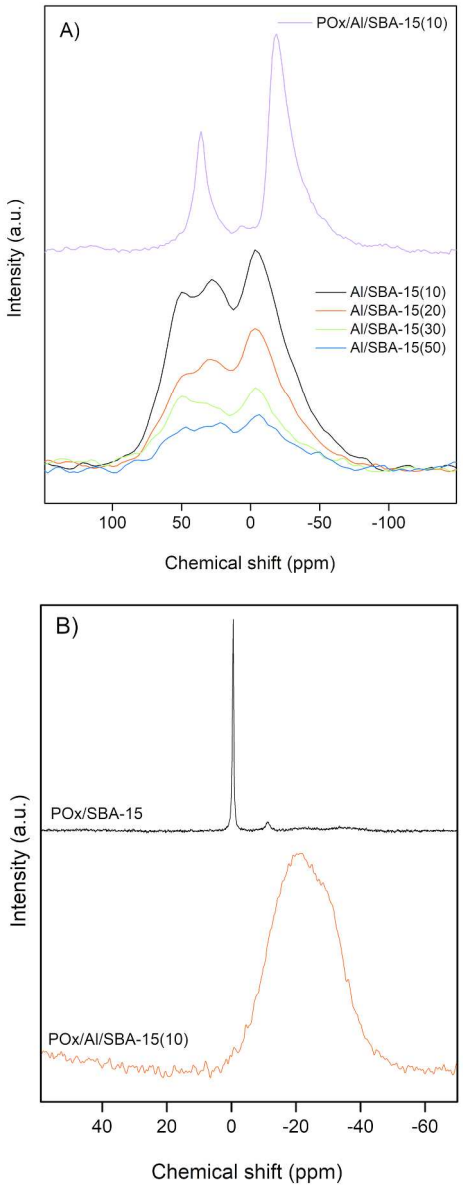

Figure 4. A) ^{27}Al MAS NMR spectra and B) ^{31}P MAS NMR spectra of the catalysts.

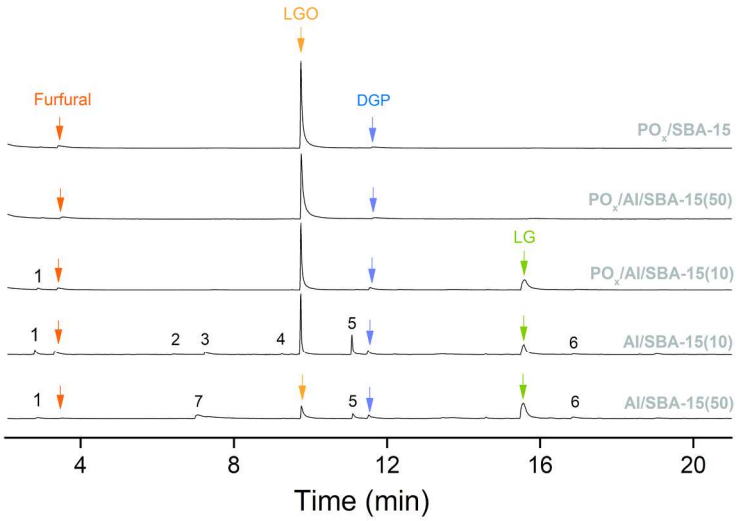

Figure 5. Total ion chromatograms of selected samples. Ref.: (1), 2(5H)-Furanone; (2), 2(3H)-Furanone, 3-acetyldihydro-; (3), 2,4(3H,5H)-Furandione, 3-methyl-; (4), 2,5-Dimethyl-4-hydroxy-3(2H)-furanone; (5), unidentified; (6), 1,6-Anhydro-β-D-glucofuranose.

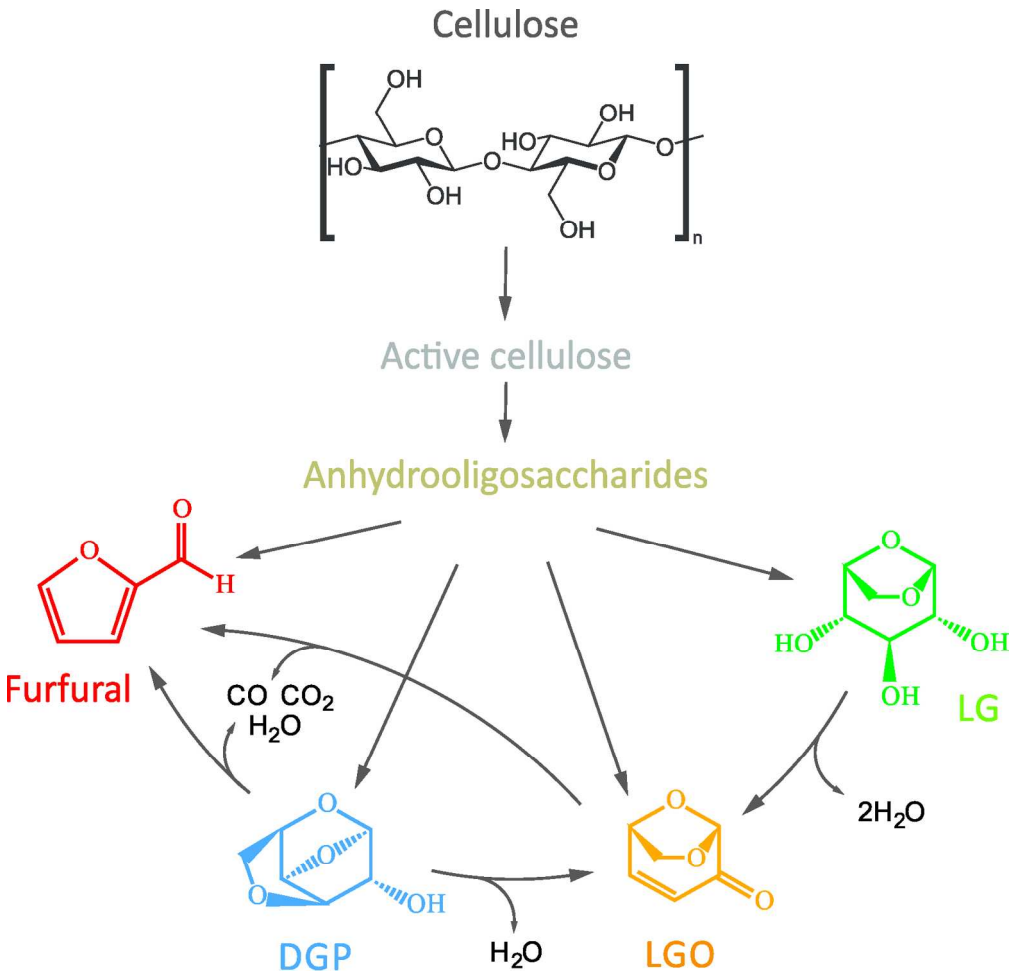

Figure 6. Reaction scheme for cellulose decomposition to condensable volatile products in the presence of Al/SBA-15 and POx/Al/SBA-15 catalysts.

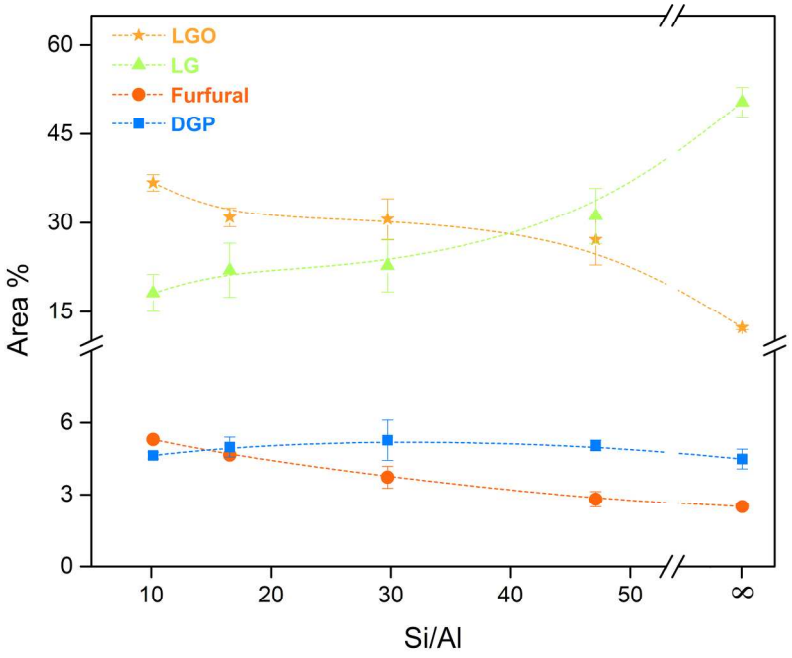

Figure 7. Volatile products selectivity as a function of Al content in Al/SBA-15 samples.

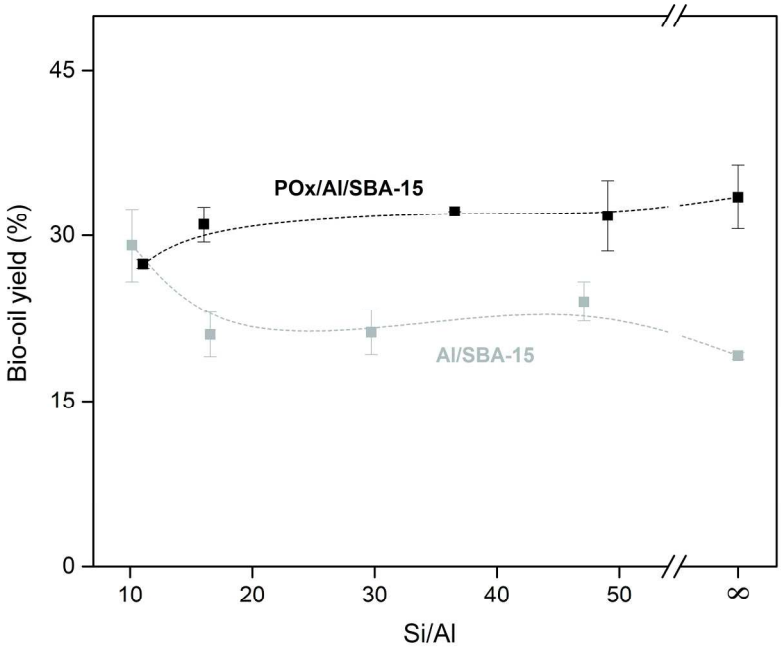

Figure 8. Bio-oil yield as a function of Si/Al ratio in the catalysts.

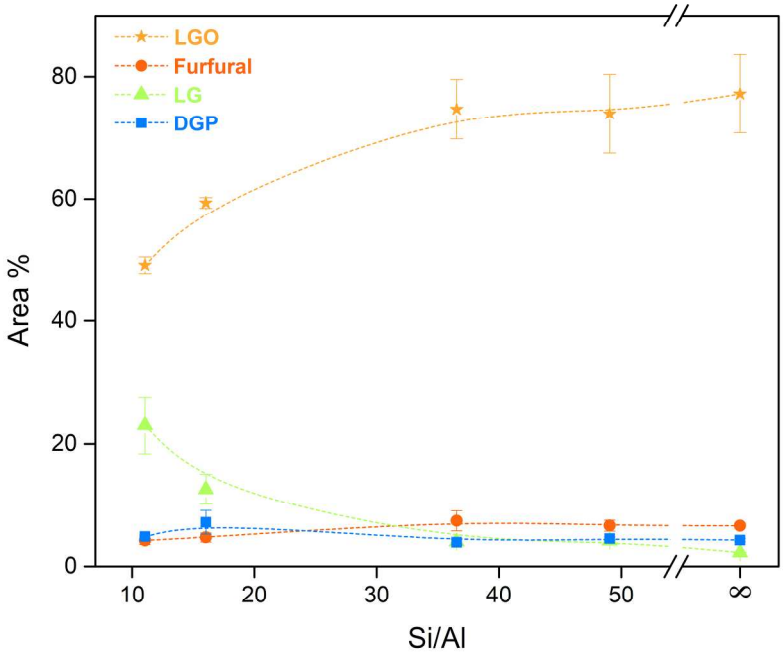

Figure 9. Volatile products selectivity as a function of Al content in POx/Al/SBA-15 solid phosphoric acid catalysts.

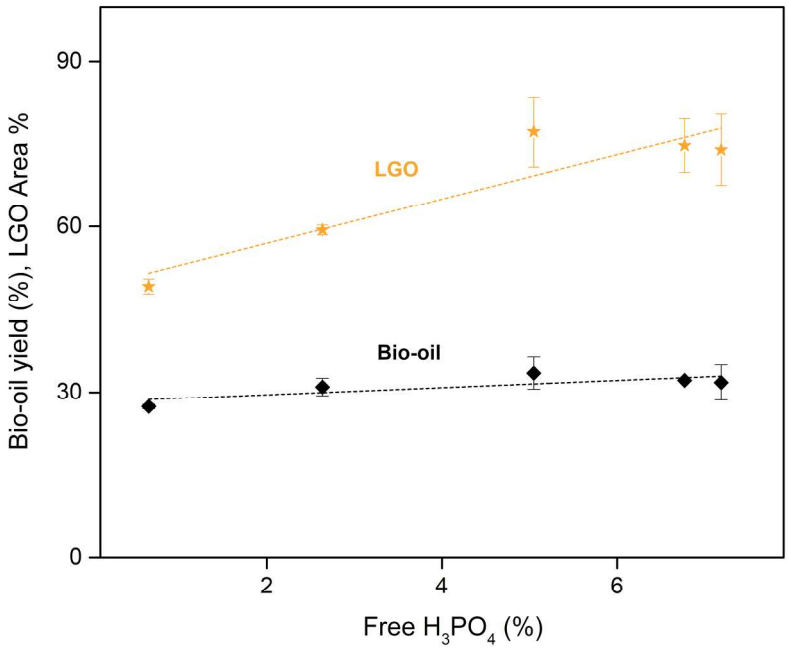

Figure 10. Levoglucosenone area % and yield to bio-oil as a function of free phosphoric acid for POx/Al/SBA-15 catalysts.

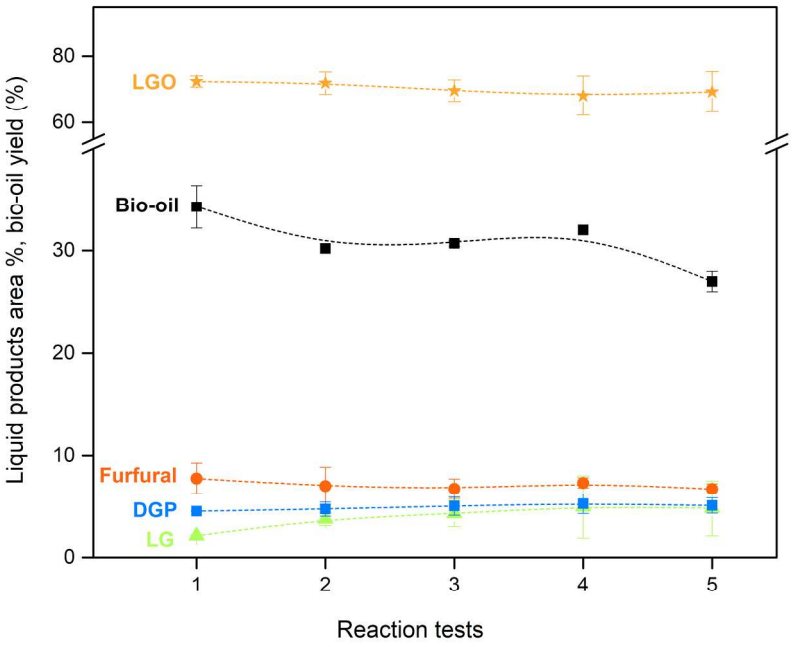

Figure 11. Volatile products distribution and bio-oil yield for PO_x/SBA-15 solid phosphoric acid catalyst during consecutive fast pyrolysis runs.